

# Optimizing the Source Distribution in Fluid Mixing

Jean-Luc Thiffeault\* and G. A. Pavliotis†

*Department of Mathematics, Imperial College London, SW7 2AZ, United Kingdom*

A passive scalar is advected by a velocity field, with a nonuniform spatial source that maintains concentration inhomogeneities. For example, the scalar could be temperature with a source consisting of hot and cold spots, such that the mean temperature is constant. Which source distributions are best mixed by this velocity field? This question has a straightforward yet rich answer that is relevant to real mixing problems. We use a multiscale measure of steady-state enhancement to mixing and optimize it by a variational approach. We then solve the resulting Euler–Lagrange equation for a perturbed uniform flow and for simple cellular flows. The optimal source distributions have many broad features that are as expected: they avoid stagnation points, favor regions of fast flow, and their contours are aligned such that the flow blows hot spots onto cold and vice versa. However, the detailed structure varies widely with diffusivity and other problem parameters. Though these are model problems, the optimization procedure is simple enough to be adapted to more complex situations.

## I. INTRODUCTION

Consider a passive scalar advected by a velocity field, in the presence of an inhomogeneous spatial source. An obvious question is, which velocity fields are best at homogenizing the concentration field? This is a challenging question, and here we turn it around into a less obvious one: given a velocity field, which source distributions are best mixed by this field? For example, in a room with a given airflow, where to best position heating units to achieve a homogeneous temperature? We will see that answering this type of question gives considerable insight into optimal stirring flows in general.

To carry out the optimization we need to narrow the problem further. First, we fix the amplitude of the velocity field, such as by specifying its total energy (in a bounded domain) or energy density (in an unbounded domain). Second, we restrict the source and velocity fields to be time-independent, so that the problem is steady. Finally, and most importantly, we need to specify how we measure the mixing enhancement due to stirring. Here we use a generalization of the variance of the concentration field, which has long been a popular measure of mixing. The reasoning is that a velocity field that is efficient at stirring should suppress fluctuations in the concentration field, and the variance decreases as these fluctuations become smaller.

Previous work on optimization of mixing has focused on breaking flow symmetries [1–4], or optimizing quantities associated with chaotic advection, such as Lyapunov exponents or topological entropy [5–10]. Recent work has also involved optimizing the norm of the concentration field [11, 12], in a manner similar to here. However, all these approaches differ from our work in that they do not involve body sources of scalar continually replenishing the variance of the concentration field. The optimal solutions we find are quite different, especially in that they do not tend to lead to creation of small spatial scales in the concentration field, but rather magnify the importance of efficient transport of temperature from sources to sinks.

Motivated by Doering and Thiffeault [13] and Shaw *et al.* [14], we introduce a one-parameter

---

\*Electronic address: jeanluc@imperial.ac.uk

†Electronic address: g.pavliotis@imperial.ac.uk

family of measures of mixing. The *mixing enhancement factor*  $\mathcal{E}_p$  is thus defined by

$$\mathcal{E}_p := \frac{\|(-\Delta)^{p/2}\tilde{\theta}\|_2}{\|(-\Delta)^{p/2}\theta\|_2}, \quad (1)$$

where  $\theta(\mathbf{x})$  is the concentration of the advected scalar,  $\|\cdot\|_2$  is the  $L^2$  norm, and  $\Delta$  the Laplacian. The  $\tilde{\theta}(\mathbf{x})$  in the numerator is the reference concentration obtained for the same source distribution and diffusivity, but in the absence of stirring. The enhancement factor thus tells us how much better the velocity field is at suppressing fluctuations than if we didn't stir at all. The above definition is appropriate for the steady advection–diffusion problem that we consider in this paper. The relevant definition for the time-dependent problem is given in Doering and Thiffeault [13], and involves taking the long-time average of the numerator and denominator in (1). As mentioned above, for simplicity we shall restrict our study to time-independent flows and sources, though the more general formulation is not conceptually more complicated. We assume without loss of generality that the source and initial condition, and consequently the scalar concentration, have spatial-mean zero. For concreteness, we will often refer to  $\theta$  as ‘temperature’ or ‘heat’, and speak of ‘hot’ and ‘cold’ regions, but the considerations here apply to any passive scalar.

The numerator in the definition of the enhancement (1) is designed to avoid pathological solutions, such as ones that concentrate the source at very small scales. Nevertheless, our definition (1) sometimes behaves counterintuitively: for instance, the enhancement can be increased by rearranging the source on large scales to penalize diffusion. These cases are not the most relevant ones, and do not justify introducing a new definition of the enhancement from that used previously Doering and Thiffeault [13], Shaw *et al.* [14], Thiffeault *et al.* [15]. Moreover, the definition (1) is well-suited to optimizing the velocity field for a fixed source distribution, which is a more important (and much more difficult) problem for which partial results are available. Keeping the same definition allows comparison to these earlier results.

For  $p = 0$ , the enhancement factor (1) involves the scalar variance and was introduced by Thiffeault *et al.* [15]. Varying  $p$  preferentially weighs the smaller ( $p > 0$ ) or larger ( $p < 0$ ) scales, providing a different measure of mixing enhancement. This measure of mixing efficiency was used by Doering and Thiffeault [13] and Shaw *et al.* [14] in the context of statistically-steady turbulent flows, and they found that the scaling of the enhancement factor with the energy of the velocity field depends strongly on the nature of the source. For  $p = -1$ , the enhancement factor is closely related to the mix-norm [11, 12].

In this paper we maximize (1) using a variational approach (Section II). The variation leads to an Euler–Lagrange equation where the leading eigenvalue is the optimal enhancement factor, with the corresponding eigenfunction giving the optimal source distribution. Some salient features of the optimal solutions are that (i) the optimal source distribution avoids having hot or cold spots over stagnation points of the flow; (ii) regions of high velocity are favored; and (iii) the hot and cold spots are positioned such that the flow sweeps hot onto cold and vice versa. Though most solutions have these broad features, they differ considerably in their details and often change dramatically (but continuously) as parameters, such as the diffusivity or the exponent  $p$  in (1), are varied.

We illustrate the range of solutions by considering first the simplest situation, that of a uniform velocity field, as discussed in Plasting and Young [16], Doering and Thiffeault [13], and Shaw *et al.* [14]. In that case the optimization problem can be solved analytically (Section III). We then impose a perturbation to the uniform flow, leading to either a shear flow or a wavy flow, and solve for the optimal source using perturbation theory. The resulting optimal sources favor regions of high velocity in the shear flow, but the wavy flow leaves the optimal solution unchanged from the uniform flow, and only decreases its efficiency. This shows, unsurprisingly, that it is still possible to improve the enhancement factor after optimizing the source by optimizing the velocity field.

We then move to direct numerical solution of the optimization problem for a simple cellular flow (Section IV). The basic problem turns out to be doubly-degenerate in that there are two independent source distributions that give the same optimal enhancement. This is a consequence of a symmetry of the flow, and we verify that breaking this symmetry by adding a small perturbation to the velocity field selects a unique optimal solution. We also use the cellular flow to study the range of behavior as the diffusivity and the exponent  $p$  in (1) are varied. In all these cases, the optimal source distribution converges at extreme parameter values (large or small diffusivity or  $p \rightarrow \pm\infty$ ). For all the cases, we also compare the optimized enhancement factor to two simple reference sources,  $\sin x$  and  $\cos x$ , chosen to capture the spatial-phase dependence of the optimal source distribution. Because of the phase of the rolls, the  $\cos x$  is much more efficient than  $\sin x$ , and its enhancement factor is very close to optimal. This is not in itself a drawback, since it shows that our definition of enhancement is fairly robust to changes in the source, a desirable feature for practical implementation. Finally, we offer some concluding remarks in Section V.

## II. THE OPTIMIZATION PROCEDURE

We consider the time-independent advection–diffusion equation for a passive scalar with concentration  $\theta(\mathbf{x})$ , spatial source  $s(\mathbf{x})$ , and diffusivity  $\kappa$ ,

$$\mathbf{u}(\mathbf{x}) \cdot \nabla \theta - \kappa \Delta \theta = s(\mathbf{x}), \quad (2)$$

in  $[0, L]^d$  with periodic boundary conditions. The (given) velocity field  $\mathbf{u}(\mathbf{x})$  is incompressible,  $\nabla \cdot \mathbf{u} = 0$ . Both  $\mathbf{u}(\mathbf{x})$  and  $s(\mathbf{x})$  are assumed to be sufficiently smooth. We assume that the source and initial condition have spatial mean zero, which implies that the scalar concentration also has mean zero. We remark that the solution  $T(\mathbf{x}, t)$  of the evolution problem

$$\partial_t T(\mathbf{x}, t) + \mathbf{u}(\mathbf{x}) \cdot \nabla T(\mathbf{x}, t) - \kappa \Delta T(\mathbf{x}, t) = s(\mathbf{x}),$$

converges, in the limit  $t \rightarrow +\infty$ , to the solution  $\theta(\mathbf{x})$  of the steady problem (2), the convergence being strong in  $L^2$ . Hence, for steady sources and stirrers, it is sufficient to consider the stationary problem (2).

### A. Optimal Mixing Enhancement

Our goal is to maximize the enhancement factor  $\mathcal{E}_p$  defined by (1),

$$\mathcal{E}_p^2 := \frac{\|(-\Delta)^{p/2} \tilde{\theta}\|_2^2}{\|(-\Delta)^{p/2} \theta\|_2^2},$$

where  $\tilde{\theta}$  solves equation (2) in the absence of advection,

$$-\kappa \Delta \tilde{\theta} = s, \quad (3)$$

with periodic boundary conditions on  $[0, L]^d$ . We assume that the velocity field is given. In maximizing the enhancement factor  $\mathcal{E}_p$ , we fix the  $L^2$  norm of the source and of the velocity field (or equivalently, the kinetic energy of the flow).

Define the linear operators

$$\mathcal{L} := \mathbf{u}(\mathbf{x}) \cdot \nabla - \kappa \Delta \quad \text{and} \quad \tilde{\mathcal{L}} := -\kappa \Delta,$$

from which we can write the solution to (2) and (3) as

$$\theta = \mathcal{L}^{-1}s \quad \text{and} \quad \tilde{\theta} = \tilde{\mathcal{L}}^{-1}s.$$

We can then rewrite the enhancement factor (1) as

$$\mathcal{E}_p^2 = \frac{\|(-\Delta)^{p/2}\tilde{\mathcal{L}}^{-1}s\|_2^2}{\|(-\Delta)^{p/2}\mathcal{L}^{-1}s\|_2^2} = \frac{\langle s, \tilde{\mathcal{A}}_p^{-1}s \rangle}{\langle s, \mathcal{A}_p^{-1}s \rangle}, \quad (4)$$

where the self-adjoint operators  $\mathcal{A}_p$  and  $\tilde{\mathcal{A}}_p$  are

$$\mathcal{A}_p := \mathcal{L}(-\Delta)^{-p}\mathcal{L}^*, \quad \tilde{\mathcal{A}}_p := \tilde{\mathcal{L}}(-\Delta)^{-p}\tilde{\mathcal{L}}^* = \kappa^2(-\Delta)^{2-p}, \quad (5)$$

and we have used the notation  $\langle \cdot \rangle$  to denote integration over  $[0, L]^d$ . To maximize  $\mathcal{E}_p^2$ , we compute its variation with respect to  $s$  and set it equal to zero,

$$\delta\mathcal{E}_p^2 = \frac{2}{\langle s, \mathcal{A}_p^{-1}s \rangle} \left\langle \left( \tilde{\mathcal{A}}_p^{-1}s - \mathcal{E}_p^2 \mathcal{A}_p^{-1}s \right) \delta s \right\rangle = 0, \quad (6)$$

which implies

$$\tilde{\mathcal{A}}_p^{-1}s = \mathcal{E}_p^2 \mathcal{A}_p^{-1}s, \quad (7)$$

or

$$\mathcal{A}_p \tilde{\mathcal{A}}_p^{-1}s = \mathcal{E}_p^2 s. \quad (8)$$

This is an eigenvalue problem for the operator  $\mathcal{K}_p := \mathcal{A}_p \tilde{\mathcal{A}}_p^{-1}$ . The optimal source is given by the ground state of the inverse of this operator, and the normalized variance is given by the corresponding (first) eigenvalue.

The operators  $\mathcal{A}_p^{-1}$  and  $\tilde{\mathcal{A}}_p^{-1}$  are self-adjoint from  $L^2([0, L]^d)$  to  $L^2([0, L]^d)$ ; furthermore, they are both positive operators in  $L^2([0, L]^d)$  (restricted to functions with mean zero). Consequently, the generalized eigenvalue problem (7) has real positive eigenvalues, and the eigenfunctions  $s$  and  $s'$  corresponding to distinct eigenvalues are orthogonal with respect to the weighted inner product  $(s, s') := \langle s, \tilde{\mathcal{A}}_p^{-1}s' \rangle$ .

Our goal now is to calculate the optimal source and the corresponding mixing enhancement factor for some simple velocity fields. In particular, in Section III we will consider a weakly perturbed uniform flow in two dimensions, and in Section IV we will consider cellular flows. We will be primarily concerned with the eigenvalue problem (7) or (8) for  $p = 0$ , i.e.

$$\mathcal{A}\tilde{\mathcal{A}}^{-1}s = \mathcal{E}^2 s, \quad (9)$$

with  $\mathcal{A} := \mathcal{A}_0 = \mathcal{L}\mathcal{L}^*$ ,  $\tilde{\mathcal{A}} := \tilde{\mathcal{A}}_0 = \kappa^2\Delta^2$  and  $\mathcal{E} := \mathcal{E}_0$ . Notice that the operator  $\tilde{\mathcal{A}}^{-1}$  is a diagonal operator in Fourier space with entries  $\kappa^2|\mathbf{k}|^{-4}$ , where  $\mathbf{k}$  is the wavevector. The large negative power of  $|\mathbf{k}|$  indicates that this operator acts as a low-pass filter, suppressing high frequencies. We shall return to the case  $p \neq 0$  in Section IV C.

## B. Is the Enhancement Maximal?

Before considering specific examples in Sections III and IV, let us demonstrate that the optimal solution obtained in Section II A is indeed a global maximum. We could do this using the second

variation of  $\mathcal{E}_p^2$ , but instead we proceed more directly by expanding an arbitrary source in terms of eigenfunctions  $s^{(i)}$  satisfying Eq. (7),

$$s(\mathbf{x}) = \sum_i a^{(i)} s^{(i)}(\mathbf{x}), \quad (10)$$

and inserting into expression (4) for the mixing enhancement factor,

$$\frac{\langle s \tilde{\mathcal{A}}_p^{-1} s \rangle}{\langle s \mathcal{A}_p^{-1} s \rangle} = \frac{\sum_{i,j} a^{(i)} a^{(j)} \langle s^{(i)} \tilde{\mathcal{A}}_p^{-1} s^{(j)} \rangle}{\sum_{i,j} a^{(i)} a^{(j)} \langle s^{(i)} \mathcal{A}_p^{-1} s^{(j)} \rangle} = \frac{\sum_{i,j} a^{(i)} a^{(j)} \langle s^{(i)} \tilde{\mathcal{A}}_p^{-1} s^{(j)} \rangle}{\sum_{i,j} \mathcal{E}_p^{(j)-2} a^{(i)} a^{(j)} \langle s^{(i)} \tilde{\mathcal{A}}_p^{-1} s^{(j)} \rangle}, \quad (11)$$

where we used the eigenfunction property. Now use the orthogonality property of the  $s^{(j)}$ ,  $\langle s^{(i)} \tilde{\mathcal{A}}_p^{-1} s^{(j)} \rangle = \delta_{ij}$ , and the fact that  $\mathcal{E}_p \geq \mathcal{E}_p^{(j)}$ , that is the optimal enhancement factor  $\mathcal{E}_p$  is the largest eigenvalue, to find

$$\frac{\langle s \tilde{\mathcal{A}}_p^{-1} s \rangle}{\langle s \mathcal{A}_p^{-1} s \rangle} = \frac{\sum_j (a^{(j)})^2 \langle s^{(j)} \tilde{\mathcal{A}}_p^{-1} s^{(j)} \rangle}{\sum_j \mathcal{E}_p^{(j)-2} (a^{(j)})^2 \langle s^{(j)} \tilde{\mathcal{A}}_p^{-1} s^{(j)} \rangle} \leq \frac{\sum_j (a^{(j)})^2 \langle s^{(j)} \tilde{\mathcal{A}}_p^{-1} s^{(j)} \rangle}{\sum_j \mathcal{E}_p^{-2} (a^{(j)})^2 \langle s^{(j)} \tilde{\mathcal{A}}_p^{-1} s^{(j)} \rangle} = \mathcal{E}_p^2, \quad (12)$$

which proves that  $\mathcal{E}_p$  is indeed optimal, since the enhancement factor of no other source can exceed it. This is a global argument, which relies only on the eigenvalue problem (7) providing a complete set of orthogonal eigenfunctions.

### III. UNIFORM FLOW WITH PERTURBATION

As a first test case for the optimization procedure of Section II, we consider a uniform flow (constant magnitude and direction in space). The uniform flow illustrates a fundamental mechanism involved in source optimization, as mentioned in Plasting and Young [16] and Shaw *et al.* [14]: the velocity field sweeps the hot source onto the cold sink, and vice versa. More generally, we expect that the optimal source will tend to have contours perpendicular to the flow. The uniform flow maximizes the mixing enhancement factor for a one-dimensional source, at fixed kinetic energy.

To capture another important feature of optimal sources, in Section III B we perturb the uniform flow to make either a shear flow or a wavy flow. The shear flow perturbation will show that optimal sources are localized over rapid regions of the flow. The wavy flow perturbation will show that sometimes aligning the source contours perpendicular to the flow is too ‘costly’, and the optimal solution is left unchanged from the uniform flow. The cost incurred is due to the weighting of the enhancement factor (1) by the purely-diffusive solution: a change in the source might make it more efficient, but it can also make the purely-diffusive solution more efficient, yielding no net gain.

Note that in this section we will restrict our optimization to the variance, that is with  $p = 0$  in the mixing enhancement (1). We shall return to the effect of varying  $p$  in Section IV C.

#### A. Uniform Flow

For completeness, in this short section we essentially rederive the results of Plasting and Young [16], Doering and Thiffeault [13], and Shaw *et al.* [14] on the optimality of a uniform flow. We start with a time-independent spatially uniform flow on  $[0, L]^d$ ,

$$\mathbf{u}(\mathbf{x}) = \mathbf{U}.$$

From definition (5) with  $p = 0$ , we have that

$$\mathcal{A} = \kappa^2 \Delta^2 - (\mathbf{U} \cdot \nabla)^2, \quad \tilde{\mathcal{A}} = \kappa^2 \Delta^2,$$

and

$$\mathcal{K} = \mathcal{A} \tilde{\mathcal{A}}^{-1} = I - \kappa^{-2} (\mathbf{U} \cdot \nabla)^2 \Delta^{-2},$$

Since  $\mathcal{K}$  is a differential operator with constant coefficients on a periodic domain, its eigenfunctions are easily verified to be

$$s_{\mathbf{k}}(\mathbf{x}) = \hat{s}_{\mathbf{k}} e^{i\mathbf{k} \cdot \mathbf{x}} + \text{c.c.},$$

where  $\mathbf{k}$  is the wavevector and  $\hat{s}_{\mathbf{k}}$  is a normalization constant, and the corresponding eigenvalues are

$$1 + \frac{|\mathbf{U} \cdot \mathbf{k}|^2}{\kappa^2 |\mathbf{k}|^4}.$$

We can maximize the above expression by choosing  $\mathbf{k}$  to be the shortest allowable vector parallel to the uniform flow  $\mathbf{U}$ . (Not all magnitudes and directions are allowed for wavevectors because the domain is periodic: the components of  $\mathbf{k}$  are integer multiples of  $2\pi/L$ .)

In the particular case where the uniform flow  $\mathbf{U}$  is along the  $x$ -axis,  $\mathbf{U} = U \hat{\mathbf{e}}_x$ , we have that

$$\mathcal{E} = \sqrt{1 + \frac{U^2 L^2}{4\pi^2 \kappa^2}} =: \sqrt{1 + \text{Pe}^2}$$

where we have defined the Péclet number  $\text{Pe} := UL/2\pi\kappa$ . As expected, in the limit as  $\kappa \rightarrow \infty$  ( $\text{Pe} \rightarrow 0$ ), the mixing enhancement factor converges to 1, i.e. in the large diffusivity limit the enhancement due to a flow becomes negligible. On the other hand, in the limit  $\kappa \rightarrow 0$  ( $\text{Pe} \rightarrow \infty$ ) the enhancement factor grows like  $\kappa^{-1}$ .

## B. Shear and Wavy Flows

Consider now a two-dimensional uniform flow along the  $x$ -axis perturbed by a weak flow,

$$\mathbf{u}(x, y) = U \hat{\mathbf{e}}_x + \varepsilon \mathbf{u}_1(x, y) - \varepsilon^2 \frac{\|\mathbf{u}_1\|_2^2}{2U} \hat{\mathbf{e}}_x, \quad (13)$$

with  $\varepsilon \ll 1$  and  $\langle \mathbf{u}_1 \rangle = 0$ . The second-order term is included to make  $\|\mathbf{u}\|_2 = U + O(\varepsilon^4)$ , so that we can compare the effect of the perturbed and unperturbed flows at equal amplitude. Specifically, we consider perturbations of the form

$$\mathbf{u}_1(x, y) = u_{1x}(y) \hat{\mathbf{e}}_x + u_{1y}(x) \hat{\mathbf{e}}_y,$$

which are simple to analyze but yield important insight. Because the base flow is in the  $\hat{\mathbf{e}}_x$  direction, the  $u_{1x}(y)\hat{\mathbf{e}}_x$  term is a shear flow perturbation, and the  $u_{1y}(x)\hat{\mathbf{e}}_y$  term is a wavy flow perturbation. Our goal is to obtain an asymptotic expansion for the optimal source and enhancement factor. For this we need to study perturbatively the eigenvalue problem (9), which we write as

$$\mathcal{A} \tilde{\mathcal{A}}^{-1} s = \lambda s, \quad (14)$$

with  $\mathcal{A} = \mathcal{L}\mathcal{L}^*$ ,  $\tilde{\mathcal{A}} = \tilde{\mathcal{L}}\tilde{\mathcal{L}}^* = \kappa^2\Delta^2$ , and  $\lambda = \mathcal{E}^2$ . We have that

$$\mathcal{L} = \mathcal{L}_0 + \varepsilon\mathcal{L}_1 + \varepsilon^2\mathcal{L}_2,$$

with

$$\mathcal{L}_0 = U\partial_x - \kappa\Delta, \quad \mathcal{L}_1 = \mathbf{u}_1 \cdot \nabla, \quad \mathcal{L}_2 = u_{2x}\partial_x,$$

where  $u_{2x}$  is the coefficient of the second-order term in (13). Consequently,

$$\begin{aligned} \mathcal{A} &= \mathcal{L}_0\mathcal{L}_0^* + \varepsilon(\mathcal{L}_1\mathcal{L}_0^* - \mathcal{L}_0\mathcal{L}_1) + \varepsilon^2(\mathcal{L}_2\mathcal{L}_0^* - \mathcal{L}_0\mathcal{L}_2 - \mathcal{L}_1\mathcal{L}_1) \\ &=: \mathcal{A}_0 + \varepsilon\mathcal{A}_1 + \varepsilon^2\mathcal{A}_2. \end{aligned}$$

Note that in this section the subscripts on the  $\mathcal{A}$ 's correspond to their order in  $\varepsilon$ , and not to the  $p$  subscript as in Eq. (5) (recall that  $p = 0$  for the present section). We expand  $s$  and  $\lambda$  in a power series in  $\varepsilon$ ,

$$\begin{aligned} s &= s_0 + \varepsilon s_1 + \varepsilon^2 s_2 + \dots, \\ \lambda &= \lambda_0 + \varepsilon\lambda_1 + \varepsilon^2\lambda_2 + \dots, \end{aligned}$$

insert the expansions for  $\mathcal{A}$ ,  $s$  and  $\lambda$  in equation (14), and equate like powers of  $\varepsilon$  to obtain the sequence of equations

$$\mathcal{A}_0\tilde{\mathcal{A}}^{-1}s_0 = \lambda_0 s_0, \tag{15a}$$

$$\mathcal{A}_1\tilde{\mathcal{A}}^{-1}s_0 + \mathcal{A}_0\tilde{\mathcal{A}}^{-1}s_1 = \lambda_0 s_1 + \lambda_1 s_0, \tag{15b}$$

$$\mathcal{A}_2\tilde{\mathcal{A}}^{-1}s_0 + \mathcal{A}_1\tilde{\mathcal{A}}^{-1}s_1 + \mathcal{A}_0\tilde{\mathcal{A}}^{-1}s_2 = \lambda_0 s_2 + \lambda_1 s_1 + \lambda_2 s_0. \tag{15c}$$

Consider first equation (15a), the unperturbed equation: from Section III A we have that

$$s_0 = \hat{s}_0 e^{ik_0 x} + \text{c.c.}, \quad \lambda_0 = 1 + \frac{U^2}{\kappa^2 k_0^2} = 1 + \text{Pe}^2.$$

where  $k_0 := 2\pi/L$ . We proceed now with equation (15b): multiply by  $s_0$  and integrate over  $[0, L]^2$  to obtain

$$\langle s_0 \mathcal{L}_1 \mathcal{L}_0^* \tilde{\mathcal{A}}^{-1} s_0 \rangle - \langle s_0 \mathcal{L}_0 \mathcal{L}_1 \tilde{\mathcal{A}}^{-1} s_0 \rangle + \langle s_0 \mathcal{A}_0 \tilde{\mathcal{A}}^{-1} s_1 \rangle = \lambda_0 \langle s_0 s_1 \rangle + \lambda_1 \|s_0\|_2^2. \tag{16}$$

Notice that  $\mathcal{A}_0$  is a differential operator with constant coefficients, and hence it commutes with  $\tilde{\mathcal{A}}^{-1}$ . Furthermore, both operators are self-adjoint, so that

$$\langle s_0 \mathcal{A}_0 \tilde{\mathcal{A}}^{-1} s_1 \rangle = \langle s_0 \tilde{\mathcal{A}}^{-1} \mathcal{A}_0 s_1 \rangle = \langle (\mathcal{A}_0 \tilde{\mathcal{A}}^{-1} s_0) s_1 \rangle = \lambda_0 \langle s_0 s_1 \rangle \tag{17}$$

and equation (16) simplifies to

$$\langle s_0 \mathcal{L}_1 \mathcal{L}_0^* \tilde{\mathcal{A}}^{-1} s_0 \rangle - \langle s_0 \mathcal{L}_0 \mathcal{L}_1 \tilde{\mathcal{A}}^{-1} s_0 \rangle = \lambda_1 \|s_0\|_2^2$$

leading to

$$\lambda_1 = \frac{\langle s_0 \mathcal{L}_1 \mathcal{L}_0^* \tilde{\mathcal{A}}^{-1} s_0 \rangle}{\|s_0\|_2^2} - \frac{\langle s_0 \mathcal{L}_0 \mathcal{L}_1 \tilde{\mathcal{A}}^{-1} s_0 \rangle}{\|s_0\|_2^2} = 0,$$

where the last equality follows from a straightforward calculation. This is a consequence of the invariance of the enhancement factor under reversal of the perturbation, from which all odd powers of  $\varepsilon$  in the enhancement factor will vanish.

Now we compute  $s_1$ . We set  $\lambda_1 = 0$  in equation (15b) to obtain

$$(\lambda_0 - \mathcal{A}_0 \tilde{\mathcal{A}}^{-1}) s_1 = \mathcal{A}_1 \tilde{\mathcal{A}}^{-1} s_0. \quad (18)$$

For definiteness, we specify the form of the perturbation,

$$u_{1x}(y) = \hat{u}_{1x} e^{ik_1 y} + \text{c.c.}$$

Notice that we do not yet need to specify  $u_{1y}(x)$ : it only affects the result at the next order. We look for a solution to (18) in the form of

$$s_1(x, y) = \hat{A}_{k_0 k_1} \hat{s}_0 \hat{u}_{1x} e^{i(k_0 x + k_1 y)} + \hat{B}_{k_0 k_1} \hat{s}_0 \bar{\hat{u}}_{1x} e^{i(k_0 x - k_1 y)} + \text{c.c.}, \quad (19)$$

and find

$$\hat{A}_{k_0 k_1} = \hat{B}_{k_0 k_1} = \frac{(k_0^2 + k_1^2)^2}{U^2 k_1^2 (2k_0^2 + k_1^2)} \left( 2U - i \frac{\kappa k_1^2}{k_0} \right). \quad (20)$$

Let us proceed now with the calculation of  $\lambda_2$ . We multiply (15c) by  $s_0$ , integrate over  $[0, L]^2$  and use (17) to obtain

$$\lambda_2 = \frac{\langle s_0 \mathcal{A}_2 \tilde{\mathcal{A}}^{-1} s_0 \rangle}{\|s_0\|_2^2} + \frac{\langle s_0 \mathcal{A}_1 \tilde{\mathcal{A}}^{-1} s_1 \rangle}{\|s_0\|_2^2},$$

which after substituting our solution (19)–(20) for  $s_1$  simplifies to

$$\lambda_2 = \frac{(4k_0^2 U^2 + k_1^4 \kappa^2)}{U^2 \kappa^2 k_1^2 (2k_0^2 + k_1^2)} \|u_{1x}\|_2^2 - \frac{1}{\kappa^2 k_0^2} \|u_{1y}\|_2^2.$$

We are really after the enhancement factor, which is

$$\mathcal{E} = \sqrt{\lambda_0 + \varepsilon^2 \lambda_2} + \text{O}(\varepsilon^4) = \sqrt{\lambda_0} + \varepsilon^2 \frac{\lambda_2}{2\sqrt{\lambda_0}} + \text{O}(\varepsilon^4),$$

so after putting it all together, we can write  $\mathcal{E}$  in terms of dimensionless quantities,

$$\mathcal{E} = \sqrt{1 + \text{Pe}^2} + \varepsilon^2 \frac{\text{Pe}^2}{2\sqrt{1 + \text{Pe}^2}} \left\{ \frac{(4 + \alpha^4 \text{Pe}^{-2})}{\alpha^2 (2 + \alpha^2)} \frac{\|u_{1x}\|_2^2}{U^2} - \frac{\|u_{1y}\|_2^2}{U^2} \right\} + \text{O}(\varepsilon^4), \quad (21)$$

where  $\alpha := k_1/k_0$  and recall that  $\text{Pe} = U/\kappa k_0$ .

Some observations regarding (21) are in order. First, notice that a nonzero  $u_{1x}$  (shear flow perturbation) increases the enhancement factor, while a nonzero  $u_{1y}$  (wavy flow) decreases it. Second, the form of  $u_{1y}$  is irrelevant, and it does not affect the first-order optimal source distribution. Third, in the limit of large  $\kappa$  (small  $\text{Pe}$ ), the  $\text{Pe}^{-2}$  term in (21), arising from  $\kappa^2 \Delta^2$  in  $\mathcal{A}_0$ , invalidates the expansion. We discuss each type of perturbation in turn.

Figure 1(a) shows the optimal source distribution for  $U = 1$ ,  $L = 2\pi$ ,  $\kappa = 0.01$  ( $\text{Pe} = 100$ ),  $\hat{u}_{1x} = 1/\sqrt{2}$ ,  $k_1 = 2$ ,  $\varepsilon = 0.15$ ,  $u_{1y} = 0$ . This is a shear flow, with contour lines shown in the background. The contour lines are closer together at the midpoint, indicating faster flow, since the perturbation is  $u_{1x}(y) = \sqrt{2} \cos 2y$ . Accordingly, the optimal source is localized at these points of faster flow. However, there is a limit to how localized it can get: if the source were to bunch



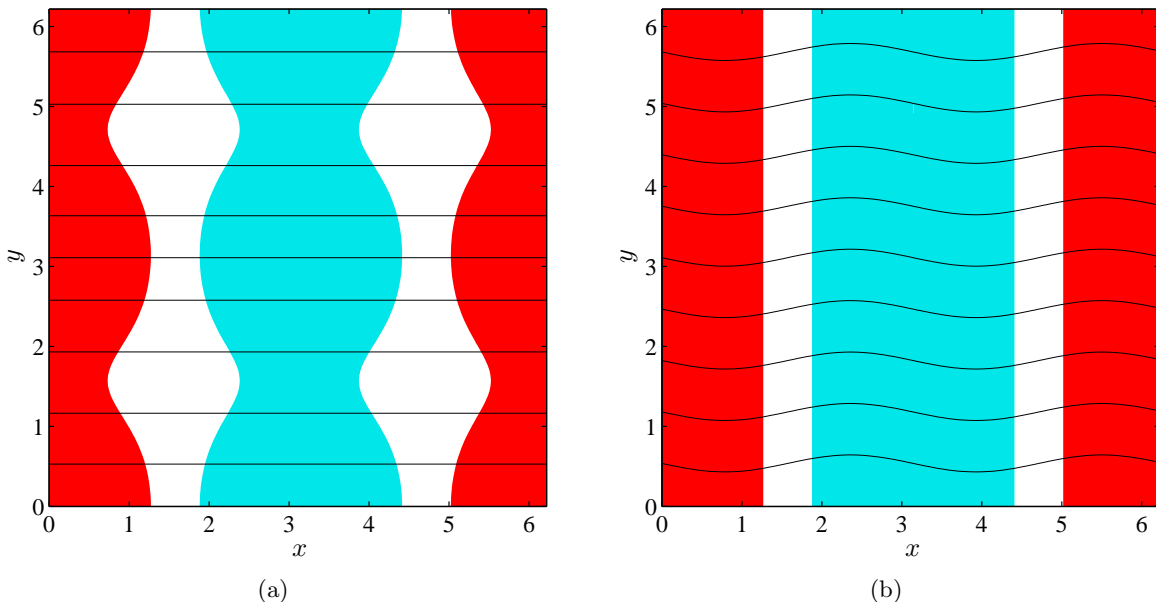


FIG. 1: Optimal source distribution for the flow  $\hat{e}_x + \varepsilon \mathbf{u}_1(x, y) - \varepsilon^2 \frac{1}{2} \|\mathbf{u}_1\|_2^2 \hat{e}_x$  with  $\varepsilon = 0.15$ ,  $\kappa = 0.01$  and (a)  $\mathbf{u}_1(y) = \sqrt{2} \cos 2y \hat{e}_x$ ; (b)  $\mathbf{u}_1(x) = \sqrt{2} \cos 2x \hat{e}_y$ . The horizontal phase of the solution is arbitrary. The background shading shows hot (red, or dark gray) and cold (blue, or light gray) regions, separated by tepid regions (white). The contour lines are streamlines of the flow.

up too much in the faster region, the purely-diffusive solution would be more effective (i.e., have lower variance), *reducing* the enhancement factor. As the perturbation gets larger, the optimal source will bunch up more in the faster regions, since the gain becomes greater. The enhancement factor is always greater than in the unperturbed case, suggesting that the advantage of faster flow regions outweighs the disadvantage of localizing the source. Finally, note that for large  $\alpha$  (large perturbation wavenumber  $k_1$ ), the mixing enhancement factor becomes independent of  $\alpha$ , reflecting the fact that a fine-scale perturbation is overwhelmed by diffusion.

Conversely, Figure 1(b) shows the optimal source distribution for the same parameters as the shear flow above but with perturbation  $u_{1y} = \sqrt{2} \cos 2x$ ,  $u_{1x} = 0$ . The streamlines in the background indicate that this is a wavy flow, with no dependence on  $y$ . The optimal source distribution, again shown in the background (here as  $\cos x$ , but the phase is arbitrary), is exactly the same as in the absence of perturbation. Intuitively, one could expect the source to be more efficient if it tilted to present its contours perpendicular to the flow, giving a wavy source. This is not the case, since the purely-diffusive solution would be more effective for a wavy source, and thus lower the enhancement factor since it enters the numerator in the definition (1). Localizing the source in regions of faster flow (as for the perturbation in Fig. 1) is a more important effect than aligning the contours of the source perpendicular to the flow.

#### IV. NUMERICAL RESULTS FOR THE CELLULAR FLOW

In Section III we derived expressions for optimal sources and mixing enhancement factors for perturbations of a uniform flow. More general velocity fields require a numerical approach. To maximize the enhancement factor, we again have to solve the generalized eigenvalue problem (8)

for the optimal source distribution  $s$ . For numerical implementation, it is preferable to solve the equivalent self-adjoint eigenvalue problem

$$(\tilde{\mathcal{A}}^{-1/2} \mathcal{A} \tilde{\mathcal{A}}^{-1/2}) r = \mathcal{E}^2 r, \quad s = \tilde{\mathcal{A}}^{1/2} r, \quad (22)$$

for the eigenvector  $r$ , which then yields the optimal source distribution  $s$ . The advantage of the form (22) is that the self-adjoint structure of the operator is explicit. In practice, we expand  $r$  as a Fourier series, so that  $\tilde{\mathcal{A}}$  is a diagonal matrix. We then solve (22) using Matlab's `eigs` routine for sparse matrices. We set the box size  $L = 2\pi$  throughout this section. Note that we shall deal only with  $p = 0$  (variance optimization) until Section IV C, so we leave off the  $p$  subscript until then.

### A. Cellular Flow

We consider the perturbed cellular flow with streamfunction

$$\psi(x, y) = A (\sin x \sin y + \delta_1 \sin 2x + \delta_2 \sin 2x \sin 2y) \quad (23)$$

with velocity field  $\mathbf{u} = (u_x, u_y) = (\partial_y \psi, -\partial_x \psi)$ , where  $A$  is a normalization constant chosen to make  $\|\mathbf{u}\|_2 = 1$ . With  $\delta_1 = \delta_2 = 0$  (the basic cellular flow), the operator  $\mathcal{L}$  is invariant under the discrete symmetry group  $\mathcal{G}$  generated by the transformations

$$G_1(x, y) = (y, -x + \pi), \quad \text{rotation with vertical translation;} \quad (24a)$$

$$G_2(x, y) = (x + \pi, y + \pi), \quad \text{diagonal translation.} \quad (24b)$$

The Abelian group  $\mathcal{G}$  has order 8 and is characterized by  $G_1^4 = G_2^2 = I$ ,  $G_1 G_2 = G_2 G_1$ .<sup>1</sup> For either  $\delta_1$  or  $\delta_2$  nonzero, the perturbations break the symmetry  $G_1$  of the cellular flow, and we shall look at their effect in turn.

First we set  $\delta_1 = \delta_2 = 0$  in (23) and solve (22) with  $\kappa = 0.01$ . In this case, there are two independent optimal source eigenfunctions with degenerate enhancement factor  $\mathcal{E} = 87.34$ , shown in Fig. 2. In the foreground are contour lines of the streamfunction. Any superposition of the two eigenfunctions in Fig. 2 will give the same enhancement factor. The degeneracy is a consequence of the symmetry  $G_1$  of the cellular flow: indeed, the two eigenfunctions are related to each other (up to a sign) by the transformation (24a). The two eigenfunctions also separately have the  $G_2$  symmetry. This situation, where the eigenfunctions corresponding to the same eigenvalue are related by a unitary representation of the symmetry group of an operator, is familiar from quantum mechanics [17, 18].

For comparison, the enhancement factor for the same flow but with the reference source  $s(\mathbf{x}) = \sin x$  is 50.01, and with the reference source  $\cos x$  is 86.61. Hence, for  $\sin x$  the optimal source gives a 74.7% improvement in the enhancement factor, but only 0.9% for  $\cos x$ . It is remarkable how close  $\cos x$  comes to the optimal enhancement factor, which shows that the optimal source is rather 'robust', so that small changes in its shape do not lead to huge changes in the enhancement factor. From a design standpoint, this is highly desirable. Table I summarizes the optimal enhancement factor results for different values of the perturbations  $\delta_1$  and  $\delta_2$ .

How to interpret the optimal source distribution in Fig. 2? The lesson learned from the uniform flow of Section III is that, ideally, the source should be such that the velocity field advects heat from hot to cold and vice versa. This is clearly happening in Fig. 2 to some extent, since in both eigenfunctions the hot and cold spots are situated such that the rolls easily advect heat between

<sup>1</sup>  $\mathcal{G}$  is the direct product of a cyclic group of order 4 and a cyclic group of order 2.

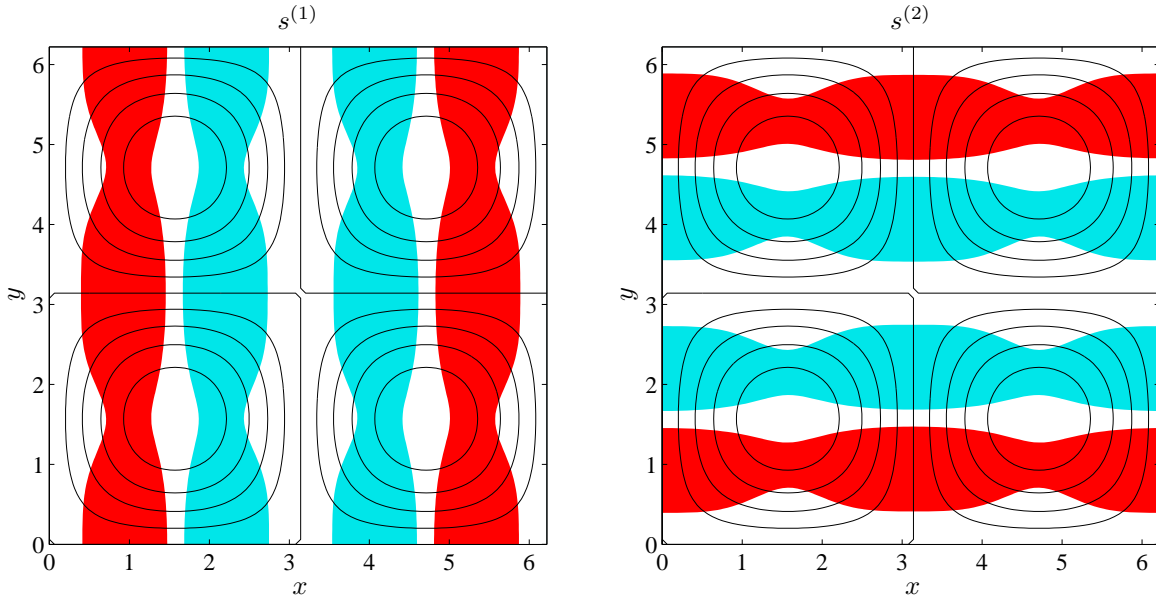


FIG. 2: Optimal source distributions for the pure cellular flow (23) with  $\delta_1 = \delta_2 = 0$ . The two pictures show degenerate orthogonal eigenfunctions with enhancement factor  $\mathcal{E} = 87.34$ . Note how there is no source of heat over the stagnation points. (See the caption to Fig. 1 for a key to the background shading.)

TABLE I: Optimal mixing enhancement factors  $\mathcal{E}_{\text{optimal}}$  with  $p = 0$  for the perturbed cellular flow (23), with  $\kappa = 0.01$ . Compare to the reference enhancements for a  $\sin x$  and  $\cos x$  source distribution: the number in parentheses is the % improvement of the optimal source. The  $\cos x$  source always does much better than  $\sin x$  because it straddles the rolls, whereas  $\sin x$  has hot and cold segregated into different rolls.

$\delta_1$	$\delta_2$	$\mathcal{E}_{\text{optimal}}$	$\mathcal{E}_{\sin}$ (%)	$\mathcal{E}_{\cos}$ (%)	note
0	0	87.34	50.01 (74.7%)	86.61 (0.9%)	Fig. 2 (degenerate)
0.05	0	87.59	49.76 (76.0%)	86.18 (1.6%)	Fig. 4(a)
0	0.05	90.10	50.26 (79.3%)	86.47 (4.2%)	Fig. 4(b)
0.05	0.05	90.19	50.01 (80.3%)	86.04 (4.8%)	
0.2	0	90.43	46.43 (94.7%)	80.41 (12.5%)	
0	0.2	95.34	53.35 (78.7%)	84.59 (12.7%)	
0.2	0.2	97.60	50.01 (95.2%)	79.30 (23.1%)	Fig. 4(c)
0.5	0	95.99	35.37 (171%)	61.25 (56.7%)	Fig. 4(d)
0	0.5	94.91	61.25 (55.0%)	79.06 (20.1%)	
0.5	0.5	106.8	50.01 (114%)	64.55 (65.4%)	

hot and cold. However, this is not the whole story: the optimal source is also distributed so as to take advantage of regions of faster flow. This is readily apparent in Fig. 3, which shows the magnitude of the velocity field in the background, and contours of the optimal source distribution from Fig. 2 (right). The hot and cold spots (elliptic regions) are clearly localized over the regions of rapid flow (pale background). Some of the fast regions appear to have no hot or cold spots, but these regions are favored in the other eigenfunction, so the symmetry is respected.

Next, we resolve the degeneracy of the optimal source distribution by setting  $\delta_1 = 0.05$  in (23) while keeping  $\delta_2 = 0$ , giving the streamfunction shown as contour lines in the foreground of

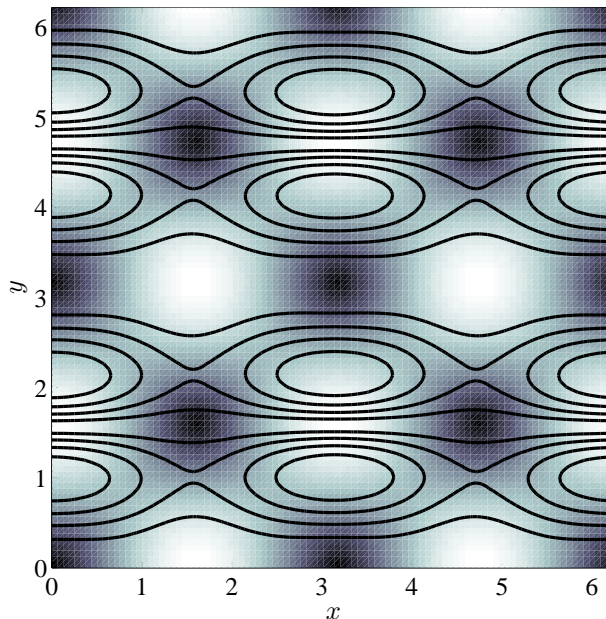


FIG. 3: The background shows the magnitude  $|\mathbf{u}|$  of the velocity field for the pure cellular flow, Eq. (23) with  $\delta_1 = \delta_2 = 0$ . The contour lines are from the optimal source distribution on the right in Fig. 2. Note how the source-sink pairs (rolls in the contours) are clustered over regions of high speed (pale) and avoid the stagnation points (dark).

Fig. 4(a). The rolls now have a slight asymmetry that breaks the rotational symmetry  $G_1$  of the unperturbed cellular flow. As a consequence, the normalized optimal eigenfunction is now unique, and is shown as the shaded background in Fig. 4(a). It is very close to the degenerate eigenfunction on the right in Fig. 2, and converges to it as  $\delta_1 \rightarrow 0$ . The enhancement factor in this case is almost unchanged, 87.59. Again, the cosine reference source has much higher enhancement factor (86.18, 1.6% improvement for the optimal source) than the sine reference source (49.76, 76.0% improvement for the optimal source).

Finally, we set  $\delta_1 = 0$  and  $\delta_2 = 0.05$  in (23), with the streamfunction shown as contours in the foreground of Fig. 4(b). As for the previous perturbation, this one also breaks the  $G_1$  symmetry and causes the optimal eigenfunction to become unique, but this time a superposition of the two degenerate eigenfunctions in Fig. 2 is selected. The optimal enhancement factor, 90.10, is again almost unchanged by this small perturbation.

To summarize this section, we presented three cases at fixed diffusivity  $\kappa = 0.01$ . The first was the cellular flow, for which we get doubly-degenerate optimal eigenfunctions. We then presented two symmetry-breaking perturbations in turn, showing how these select a particular mixture of the degenerate eigenfunctions to create a unique optimal source distribution. Since the perturbations are small, the optimal enhancement factor in all these cases is about the same, showing an improvement of about 75–80% over the reference source  $\sin x$ , but only 1–5% over the reference source  $\cos x$ . This latter modest improvement is best seen not as a failure of the optimization procedure, but as an advantage, since robustness is always desirable. In fact robustness can easily be gauged by looking at the magnitude of the next largest eigenvalues, to see how far they are from the dominant one(s). Table I also shows that the modest improvement over the cosine source is an accident, since for many other velocity fields improvements well above 50% are seen for both

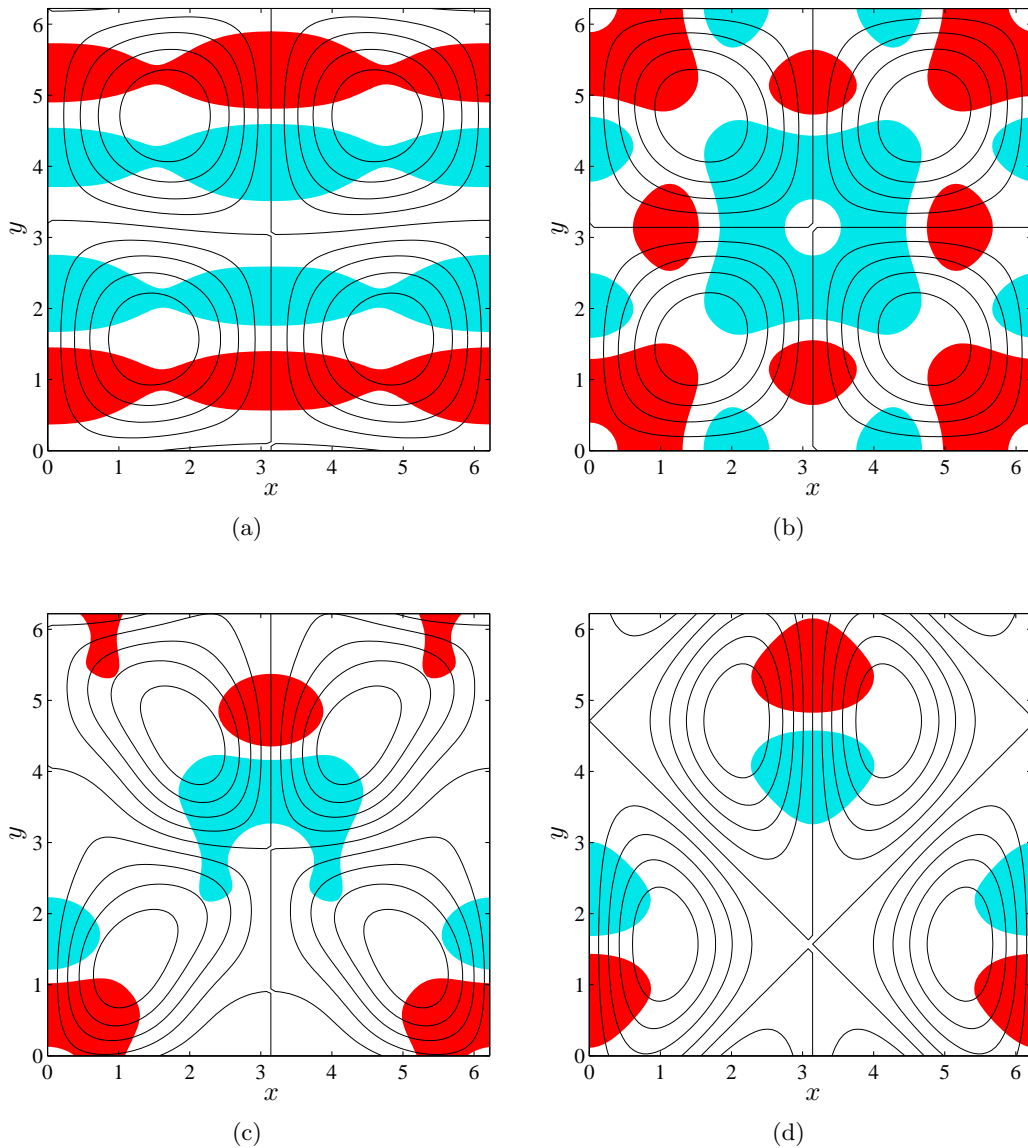


FIG. 4: Optimal source distribution for the perturbed cellular flow (23) with (a)  $\delta_1 = 0.05$ ,  $\delta_2 = 0$ , mixing enhancement factor  $\mathcal{E} = 87.59$ ; (b)  $\delta_1 = 0$ ,  $\delta_2 = 0.05$ ,  $\mathcal{E} = 90.10$ ; (c)  $\delta_1 = \delta_2 = 0.2$ ,  $\mathcal{E} = 97.60$ ; (d)  $\delta_1 = 0.5$ ,  $\delta_2 = 0$ ,  $\mathcal{E} = 95.99$ . The perturbations all break the  $G_1$  symmetry and selects a linear combination of the degenerate eigenfunction in Fig. 2. (See the caption to Fig. 1 for a key to the background shading.)

sine and cosine. Two further examples for large perturbations are shown in Figs. 4(d) and 4(c).

### B. Dependence on Diffusivity

Now we will fix  $\delta_1 = \delta_2 = 0$  in (23) and vary the diffusivity,  $\kappa$ . For  $\kappa = 0.01$ , Fig. 2 shows the two degenerate optimal source eigenfunctions, and we will follow the change in the one on the left as  $\kappa$  is varied. In Fig. 5 we show the change in the optimal source as  $\kappa$  is increased from 0.1 to 100. The optimal source distribution appears to become independent of  $\kappa$  both for small  $\kappa$  and

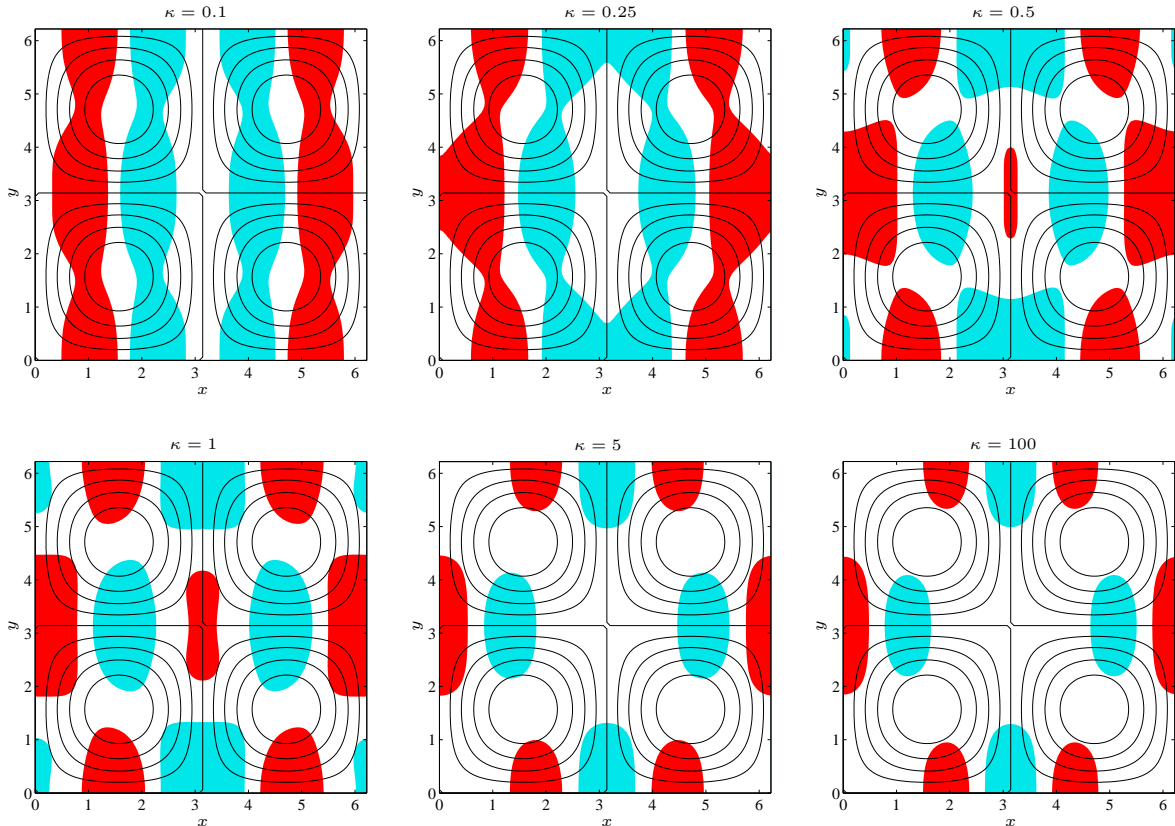


FIG. 5: For the same flow as in Fig. 2, optimal source distribution for different values of the diffusivity  $\kappa$ , increasing from top left to bottom right. The eigenfunction is doubly-degenerate and corresponds to the one on the left in Fig. 2. For both small and large  $\kappa$  the optimal source converges to an invariant eigenfunction. In all cases there is no source of temperature over the elliptic stagnation points, but in the large  $\kappa$  case there are sources and sinks over some hyperbolic points. (See the caption to Fig. 1 for a key to the background shading.)

large  $\kappa$ , but the distributions are different. The transition between the two regimes occurs when  $\kappa$  is of order unity. Though the two asymptotic sources are very different, they respect the general principles laid out in Section IV A: the source is arranged for effective transport of hot onto cold and vice versa, and regions of high speed are favored. In particular, note that the center of the rolls has a nearly zero, flat source distribution in all cases.

Another perhaps surprising aspect of the large  $\kappa$  solution in Fig. 5 is that it has complicated structure. In this large diffusivity limit, one would expect diffusion to dominate and gradients to be smoothed out. But since our mixing enhancement factor (1) compares the variance to the unstirred case, which already has very low variance, any amount of improvement will count. Hence, the complicated source for large  $\kappa$  in Fig. 5 only gives a minute improvement to the enhancement factor. The large  $\kappa$  optimal solution is particular in that it has some hot and cold spots localized over hyperbolic stagnation points. This is probably due to the high speeds along the separatrices being favored, even at the cost of straddling hyperbolic stagnation points a little.

Figure 6 shows how the mixing enhancement factor varies as a function of the diffusivity. The solid line is for the optimal source, the dashed lines for the reference sources  $\sin x$  and  $\cos x$ . For small  $\kappa$ , the enhancement factor of all sources scales as  $\kappa^{-1}$ : this is the ‘classical’ scaling discussed in [13–15], where the enhancement factor is linear in the Péclet number. It has been rigorously

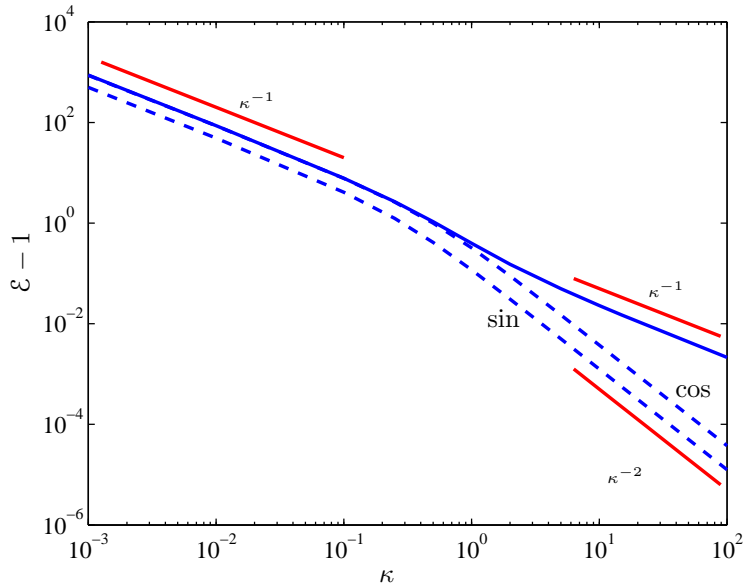


FIG. 6: For the flow with streamfunction as in Fig. 2, mixing enhancement factor  $\mathcal{E} - 1$  as a function of the diffusivity  $\kappa$ : optimal source (solid line), and  $\sin x$  and  $\cos x$  reference sources (dashed lines). For small  $\kappa$ , the enhancement factor scales like  $\kappa^{-1}$ . For large  $\kappa$ , the optimal solution returns to a  $\kappa^{-1}$  approach to unity after a brief dip, while the reference source solution approaches unity as  $\kappa^{-2}$ .

proved in [13–15] that this scaling is optimal over all possible sources and velocity fields.

For  $\kappa$  near unity, the optimal enhancement factor has a small dip before converging towards unity as  $\kappa^{-1}$  for large  $\kappa$ . In contrast, the reference enhancement factors converges to unity as  $\kappa^{-2}$ . This last scaling holds for the uniform flow of Section III when expanded in large  $\kappa$ , and is verified for other flows and sources as well [13–15].

In summary, the optimal source distribution becomes independent of  $\kappa$  for both large and small  $\kappa$ , but of course for large  $\kappa$  the efficiency gain is minimal (since the  $L^2$ -norm of the velocity is fixed). For small  $\kappa$  the efficiency gain is a constant multiple of the reference sources, but this multiple is fairly small for  $\cos x$  (1.01), showing that optimization is very robust but not necessarily always worthwhile. Overall, the optimal enhancement factor scales as  $\kappa^{-1}$ , with a momentary break in the scaling that corresponds to the complicated change in topology seen in Fig. 5 for  $\kappa$  near unity.

### C. Dependence on Exponent $p$

Our final study will be to examine the behavior of the optimal enhancement factor as  $p$  is varied in (1). In Sections IV A–IV B we used  $p = 0$ ; now we fix  $\delta_1 = \delta_2 = 0$ ,  $\kappa = 0.01$ , and allow  $p$  to vary over negative and positive values. Figure 7 shows the optimal source distributions for  $p$  varying from  $-1$  to  $2$ . For both negative and positive  $p$ , the optimal source distribution converges rapidly to invariant patterns, and the two extremes in Fig. 7 are representative of those asymptotic patterns. The situation is thus entirely analogous to the case where diffusivity was varied (Fig. 5).

The top-left picture in Fig. 7 (negative  $p$ ) shows small, localized sources and sinks. In contrast, the bottom-right picture in Fig. 7 (positive  $p$ ) shows large, regular localized sources and sinks. In fact, what is striking about the pattern is its simplicity: it is what one might take as a guess at an efficient source distribution, with no added frills. Thus, a high power of  $p$  might be useful in situations where a simple configuration is necessary due to engineering constraints. The reason

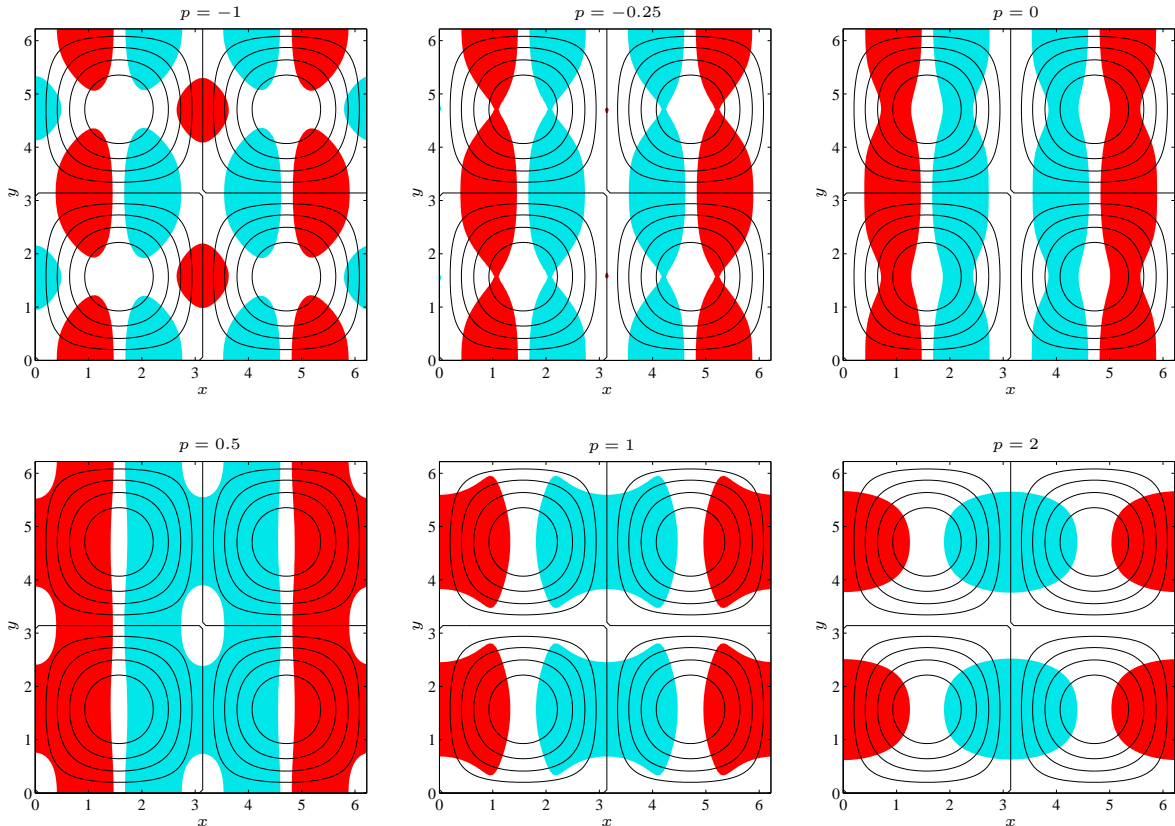


FIG. 7: For the same flow as in Fig. 2, optimal source distribution for different exponents  $p$ , increasing from top left to bottom right. The eigenfunction is doubly-degenerate and corresponds to the one on the left in Fig. 2. For both small and large  $p$  the optimal source converges to an invariant eigenfunction. In all cases there are no sources or sinks of temperature over the stagnation points. (See the caption to Fig. 1 for a key to the background shading.)

for the simplicity is that spatial variations in the source favor the diffusion operator in  $\mathcal{L}$ , and as  $p \rightarrow \infty$  these are magnified. Thus, the source must remain as spatially simple as possible while trying to maximize alignment with the velocity. As  $p \rightarrow -\infty$ , spatial variations of the source are downplayed by the norm, allowing more complexity.

Figure 8 shows how the optimal mixing enhancement factor varies as a function of  $p$ . For  $p \rightarrow -\infty$ , the enhancement factor goes to infinity, as does the enhancement factor of the two reference sources. For  $p \rightarrow \infty$ , the enhancement factor also goes to infinity, but the reference source enhancement factors now approach constants (the constant is 1 for  $\sin x$ ). Again, we are seeing the effect of the diffusion term dominating when gradients are present, since these are amplified by  $(-\Delta)^{p/2}$ . Note that the curve is symmetric about  $p = 1$ , which leads to a minimum there: whether this is true in general has not been determined, but we have not found a counterexample. In Appendix A we provide a partial proof by explicitly finding the symmetry between the operators  $\mathcal{A}_{2-p}$  and  $\mathcal{A}_p$ , but only for large  $\kappa$ .



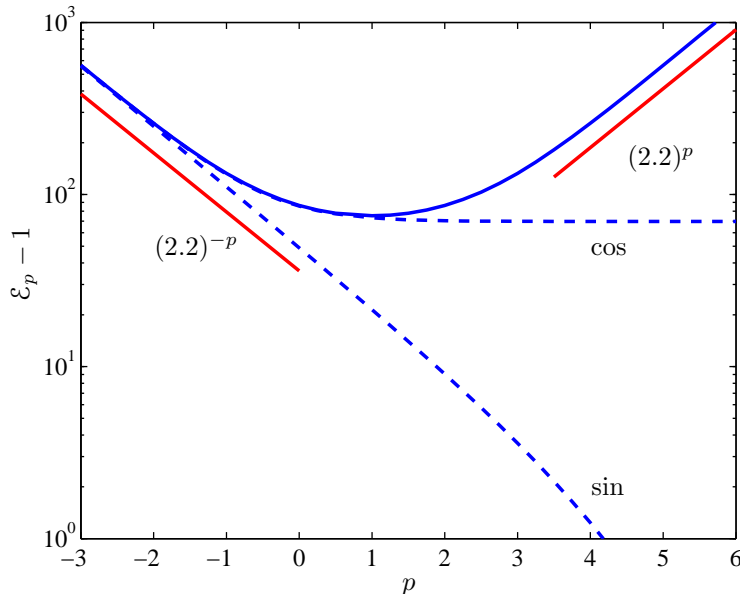


FIG. 8: For the flow with streamfunction as in Fig. 2, mixing enhancement factor  $\mathcal{E}_p - 1$  as a function of the exponent  $p$ : optimal source (solid line), and  $\sin x$  and  $\cos x$  reference sources (dashed line). The optimal enhancement factor is symmetric about  $p = 1$ , and for  $|p| \gg 1$  it grows as  $(2.2)^{|p|}$ .

## V. DISCUSSION

In both the perturbation problem (Section III) and the numerical examples (Section IV), the optimal source distributions tend to exhibit the following features:

1. Avoidance of stagnation points of the flow, especially of elliptic type;
2. Localization over regions of rapid flow;
3. Alignment of the source contours perpendicular to the local velocity, so that hot is swept onto cold and vice versa.

For a shear flow perturbation (Section III B), the optimal source bulges out over regions of faster flow. In contrast, a wavy flow perturbation leaves the optimal source unchanged over from a uniform flow, suggesting that localization is a more important effect than alignment. This also demonstrates that the optimal solution for source optimization does not necessarily correspond to the optimal solution for velocity optimization, given that optimal source. This is because at fixed energy the wavy flow always decreases the optimal enhancement factor from that of the uniform flow, for the same source distribution.

These considerations show that the mixing enhancement factor and optimization procedure described in this paper (Section II) behave in a natural manner. Furthermore, the procedure yields a global maximum (Section II B), is numerically well-behaved, and is easy to implement. Indeed, a three-dimensional application to a real system is well within the realm of feasibility: the examples we presented here (except for the uniform flow) were two-dimensional, but for smooth flows the sparse nature of the advection-diffusion operator in Fourier space means that large problems can be solved with a modest amount of computer power and memory.

The optimal source distribution becomes independent of the diffusivity  $\kappa$  for both large and small  $\kappa$  (Section IV B), and for exponent  $p$  [see Eq. (1)] negative and large or positive and large

(Section IV C). None of the source distributions achieved in these cases resemble each other. However, we observed that the eigenvalue spectrum of (7) is always symmetric about  $p = 1$  (and has a minimum there), which implies that the operators (and thus the optimal source distributions) are related by a unitary transformation we were unable to find in general (but see Appendix A for a partial result). The large positive  $p$  case is particularly interesting, since it favors source distributions that are very smooth, a desirable feature in practical applications. Another attractive feature we observed is the robustness of the optimal solution in the cases considered (Section IV A), but this will not necessarily hold in general.

To widen the applicability of the procedure, a few complications will have to be introduced. First, time-dependence of the flow and the source is desirable, which will make the variational problem more difficult to solve in principle. Second, and more importantly, there remains the much more difficult problem of optimizing the velocity field given a source distribution. The variational problem is easily formulated, but does not present itself in the nice generalized eigenvalue problem [Eq. (7)] we saw here. The third and ultimate goal is a full dynamical coupling to the Navier–Stokes equation, with buoyancy and other effects included as appropriate.

Throughout the paper we spoke of ‘mixing’ because our description involves the interplay of stirring and molecular diffusion. However, we highlighted the more interesting limit of small diffusivity  $\kappa$  (large Péclet), since this is the situation in which stirring is more pertinent. In that case, it is clear that the pushing of hot fluid onto cold regions and vice versa is better described as ‘transport’ rather than ‘mixing’. Thus, perhaps in that limit we should speak of a ‘transport enhancement factor’, but since our analysis applies even for very large  $\kappa$  we have kept the terminology, in spite of the fact that the velocity fields presented here do not lead to creation of small scales and thus may not ‘mix’ very well by some criteria.

### Acknowledgments

The authors thank Charles R. Doering for inspiring discussions. J.-L.T. was supported in part by the UK Engineering and Physical Sciences Research Council grant GR/S72931/01.

- 
- [1] J. G. Franjione and J. M. Ottino, ‘Symmetry concepts for the geometric analysis of mixing flows,’ *Philosophical Transactions: Physical Sciences and Engineering* **338** (1650), 301–323 (1992).
  - [2] R. O. Grigoriev, ‘Chaotic mixing in thermocapillary-driven microdroplets,’ *Phys. Fluids* **17**, 033601 (2005).
  - [3] I. Mezić and S. Wiggins, ‘On the integrability and perturbation of three-dimensional fluid flows with symmetry,’ *J. Nonlinear Sci.* **4** (2), 157–194 (1994).
  - [4] T. H. Solomon and I. Mezić, ‘Uniform resonant chaotic mixing in fluid flows,’ *Nature* **425**, 365–380 (2003).
  - [5] D. D’Alessandro, M. Dahleh, and I. Mezić, ‘Control of mixing in fluid flow: A maximum entropy approach,’ *IEEE Transactions on Automatic Control* **44** (10), 1852–1863 (1999).
  - [6] A. Balogh, O. M. Aamo, and M. Krstic, ‘Optimal mixing enhancement in 3-d pipe flow,’ *IEEE Trans. Control Sys. Tech.* **13**, 27–41 (2005).
  - [7] A. Vikhansky, ‘Enhancement of laminar mixing by optimal control methods,’ *Chem. Eng. Sci.* **57** (14), 2719–2725 (2002).
  - [8] J.-L. Thiffeault and M. D. Finn, ‘Topology, braids, and mixing in fluids,’ *Phil. Trans. R. Soc. Lond. A* **364**, 3251–3266 (2006).
  - [9] A. Sharma and N. Gupte, ‘Control methods for problems of mixing and coherence in chaotic maps and flows,’ *Pramana – Journal of Physics* **48**, 231–248 (1997).

- [10] B. R. Andrievskii and A. L. Fradlov, ‘Control of chaos: Methods and applications. II. Applications,’ *Autom. Remote Control* **65** (4), 505–533 (2004).
- [11] G. Mathew, I. Mezić, and L. Petzold, ‘A multiscale measure for mixing,’ *Physica D* **211** (1-2), 23–46 (2005).
- [12] G. Mathew, I. Mezić, S. Grivopoulos, U. Vaidya, and L. Petzold, ‘Optimal control of mixing in Stokes fluid flows,’ *J. Fluid Mech.* (2007), in press.
- [13] C. R. Doering and J.-L. Thiffeault, ‘Multiscale mixing efficiencies for steady sources,’ *Phys. Rev. E* **74** (2), 025301(R) (2006).
- [14] T. A. Shaw, J.-L. Thiffeault, and C. R. Doering, ‘Stirring up trouble: Multi-scale mixing measures for steady scalar sources,’ *Physica D* **231** (2), 143–164 (2007).
- [15] J.-L. Thiffeault, C. R. Doering, and J. D. Gibbon, ‘A bound on mixing efficiency for the advection–diffusion equation,’ *J. Fluid Mech.* **521**, 105–114 (2004).
- [16] S. Plasting and W. R. Young, ‘A bound on scalar variance for the advection–diffusion equation,’ *J. Fluid Mech.* **552**, 289–298 (2006).
- [17] E. P. Wigner, *Group theory and its application to the theory of atomic spectra* (Academic Press, New York, 1959).
- [18] M. Hamermesh, *Group Theory and its Application to Physical Problems* (Dover, New York, 1989).

### APPENDIX A: SYMMETRY OF OPTIMAL MIXING ENHANCEMENT FACTOR ABOUT $p = 1$

In this appendix we will motivate the symmetry of the optimal enhancement factor curve about  $p = 1$ , as evident in Fig. 8. We use the self-adjoint form (22): let

$$\mathcal{B}_p[\mathbf{u}] := \tilde{\mathcal{A}}_p^{-1/2} \mathcal{A}_p[\mathbf{u}] \tilde{\mathcal{A}}_p^{-1/2},$$

where we have explicitly shown the dependence of the operators on  $\mathbf{u}(\mathbf{x})$ . We show below that

$$\mathcal{P} \mathcal{B}_{2-p}[\mathbf{u}] \mathcal{P} = \mathcal{B}_p[\mathcal{P}\mathbf{u}] + \mathcal{O}(\kappa^{-2}), \quad (\text{A1})$$

where  $\mathcal{P}$  is the parity change operator, defined by  $\mathcal{P}r(\mathbf{x}) = r(-\mathbf{x})$  and  $\mathcal{P}\mathbf{u}(\mathbf{x}) = -\mathbf{u}(-\mathbf{x})$ , with  $\mathcal{P}^{-1} = \mathcal{P}$ . Since the spectrum is unchanged by the substitution  $\mathbf{u}(\mathbf{x}) \rightarrow -\mathbf{u}(-\mathbf{x})$ , establishing (A1) proves that  $\mathcal{B}_{2-p}[\mathbf{u}]$  and  $\mathcal{B}_p[\mathbf{u}]$  have the same spectrum, which explains the symmetry of the enhancement factor about  $p = 1$ . The eigenfunctions are related by a parity change. Unfortunately, Eq. (A1) is only an asymptotic result valid for large  $\kappa$ , and we do not know the general form of the symmetry  $\mathcal{P}$  for smaller  $\kappa$ , though numerical evidence suggests it exists.

To show (A1) directly, we expand

$$\mathcal{P} \mathcal{B}_{2-p}[\mathbf{u}(\mathbf{x})] \mathcal{P} = 1 + \kappa^{-1} \left( (-\Delta)^{-\frac{p}{2}} \mathcal{P}\mathbf{u}(\mathbf{x}) \cdot \nabla \mathcal{P} (-\Delta)^{\frac{p}{2}-1} - (-\Delta)^{\frac{p}{2}-1} \mathcal{P}\mathbf{u}(\mathbf{x}) \cdot \nabla \mathcal{P} (-\Delta)^{-\frac{p}{2}} \right) + \mathcal{O}(\kappa^{-2})$$

where we used the commutativity of  $\Delta$  and  $\mathcal{P}$ . We also have

$$\mathcal{B}_p[-\mathbf{u}(-\mathbf{x})] = 1 + \kappa^{-1} \left( (-\Delta)^{-\frac{p}{2}} \mathbf{u}(-\mathbf{x}) \cdot \nabla (-\Delta)^{\frac{p}{2}-1} - (-\Delta)^{\frac{p}{2}-1} \mathbf{u}(-\mathbf{x}) \cdot \nabla (-\Delta)^{-\frac{p}{2}} \right) + \mathcal{O}(\kappa^{-2}).$$

Now Eq. (A1) follows from  $\mathcal{P}\mathbf{u}(\mathbf{x}) \cdot \nabla \mathcal{P} = \mathbf{u}(-\mathbf{x}) \cdot \nabla$ , since both  $\mathbf{u}$  and  $\nabla$  reverse direction under parity change.